Titanium scaffolds fabricated by Direct Ink Writing and functionalized with dual-action coatings with osteoinductive and antibacterial properties

Diego Torres Garrido[1] diego.torres@ames.group; Jose Antonio Calero[1]. jacalero@ames.group; Jose Maria Manero[2] jose.maria.manero@upc.edu; Elisa Rupérez[2] elisa.ruperez@upc.edu
[1] AMES PM Tech Center, Camí Can U'bach, 8, 08620 Sant Vicenç dels Horts, Barcelona, Spain
[2] Universidad Politécnica de Cataluña, Av. Eduard Maristany 16. 08019 Barcelona, Spain

Abstract

The stress shielding, a result of the stiffness mismatch between titanium and bone, the lack of bioactivity and the infections are the main cause of the implants failure. In this work, porous titanium structures (between 50 and 70%) were produced by direct ink writing, using a new Ti ink formulation. A water and thermal treatment was optimized to ensure the complete elimination of the binder before the sintering process. The samples were sintered in high vacuum at 1150 ºC.The stiffness and compressive strength were similar to those of cancellous bone. The functionalization of the scaffold surface with a thermochemical treatment that incorporates Ga ions resulted in Ga-containing calcium titanate layer that generate homogeneous apatite layer in simulated body fluid. The $Ga3+$ release promote the antibacterial effect against gram positive strains. SaOS-2 cells adhered and proliferated on the Ga-doped Ti surfaces; its presence contributes to cell differentiation and increases the mineralization.

Keywords

Direct ink writing, Titanium scaffolds, Gallium, Antibacterial activity, Osseointegration

1.   Introduction

One of the main goals of the tissue engineering is the development of porous scaffolds that mimic the properties of the bone. For the manufacture of implants it is necessary that the material has an optimal biointegration, which includes a strong and stable interaction between the material and the cells. In recent years, porous structures of titanium (foams) have been studied and have shown excellent biocompatibility, mechanical properties, and a low elastic modulus that allows reducing the amount of stress shielding [1].

In this context, additive manufacturing technologies (AM), based on the layer-by-layer fabrication, have attracted much attention. The main advantage is that they allow building complex 3D structures with precise control of both the external geometry and the internal porosity [2]. Direct ink writing (DIW) is a low-cost AM technology that can be used to manufacture porous metallic structures with complex shapes and controlled geometries at the micrometer scale without wasting metal powder [3]. This technique enables the fabrication of scaffolds by extruding a metallic ink through a nozzle, obtaining the green part, and subsequently sintering treatment. This process avoids the use of a powder bed and its waste, offers the possibility to work with multimaterial inks [4], and in case that support material is needed this can be easily removed from the green part.

The importance of finding new alternatives to protect surgeries from bacteria or other microorganism infections is already well established. Around 20% of implant surgeries fail because of microbial infections and 18% due to the mechanical loosening of the implant [5]–[9]. The bioactivity of the surface is also a critical issue to ensure optimal osseointegration and full bone colonization of the 3D structure. There are several metal ions that have shown not only appealing antimicrobial effects but also to provide certain bioactivity to implant surfaces. Trivalent Gallium (Ga) presents some special properties such as an antibacterial agent [10], [11]. Furthermore, it has been proven that Ga stops bone resorption by lessening the activity of the osteoclasts, prevent bone calcium release and augment bone mass by stimulating osteoblasts activity [12]–[14].

The objectives of the present work was to develop a novel DIW process to obtain 3D titanium scaffolds for orthopedic applications and introduce Ga ions by a modification of the traditional thermochemical treatment developed by Kokubo to improve the bioactivity and achieve antibacterial response.

A physical-chemical and mechanical characterization was carried out on titanium porous samples obtained by developed method (DIW + sinter). The results were validated by comparison with OsteoSinter®, an Ames medical implant with CE mark obtained by conventional PM. The optimal gallium concentration of the thermo chemical treatment was determinate by apatite-forming ability, the evaluation of the antibacterial properties and the assessment of the osteoblastic-like cell adhesion, proliferation, differentiation and mineralization.

2. Experimental Method
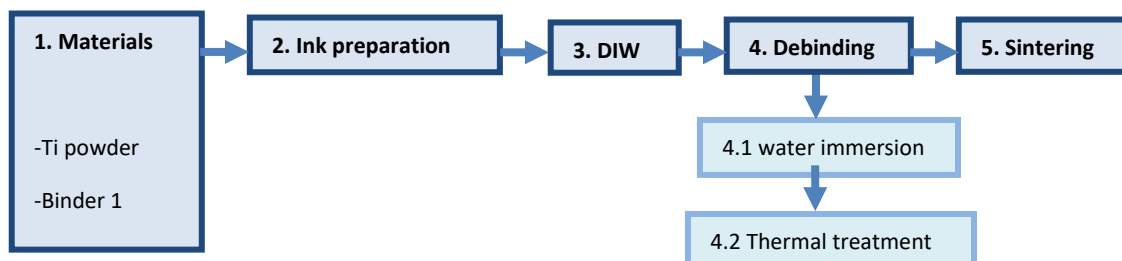
2.1 Titanium scaffold fabrication

Figure 1 Schematic process of titanium scaffold manufacturing.

Ti powder (~325 mesh, 99.5% purity, density: 4.5 g/cm3, Alfa Aesar, MA, USA) was used in this study. The morphological characterization of the Ti powder was carried out by scanning electron microscopy. The size distribution and mean size of Ti particles were characterized by laser diffraction. Thermoresponsive polymer was used as binder1 in the form of a hydrogel. It was prepared by dissolving the polymeric powder in distilled water at a concentration of 30% (w/w). Thermoplastic polymer was used as binder 2 in the form of a liquid. It was prepared by dissolving the polymeric pellets in organic solvent at a concentration of 20% (w/w). Both binders were prepared and blended using an asymmetric centrifugal mixer system (SpeedMixer DAC 150.1 FVZ, Hamm, Germany). Ti-based inks were prepared by mixing Ti powder with both binders (75% w/w titanium powder),

Slic3r software was used to define the printing parameters and generate a customized G-code. Samples were printed using a customized DIW device (BCN3D+ Dual Paste Extruder, Fundació CIM, Spain). The nozzle size was 410 µm (Smooth Flow Tapered Tips, Nordson EFD) and the layer height was set to 350 µm. The infill density was 30, 40 and 50% (70, 60 and 50% of porosity) in order to evaluate the effect of the porosity. The ink was introduced in a 3 cm3 syringe (Optimum, Syringe Barrels, Nordson EFD), with the nozzle mentioned above and the whole assembly was installed into the DIW device.
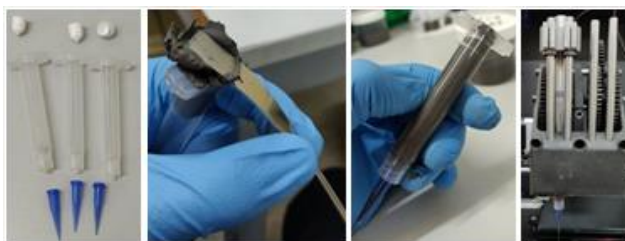

Figure 2 Direct ink writing preparation and printer device.

Thermal characterization of the ink was performed by thermogravimetric analysis (TGA) in order to determine the optimal protocol for binder removal. In order to confirm the elimination of the binder, the carbon and oxygen contents of treated samples were analyzed by using a LECO CS-200 carbon analyzer and LECO ON736 oxygen analyzer.

Following the binder removal treatment, the scaffolds were sintered at 1150◦C and 1350◦C, in a tubular furnace, under high vacuum 10-5mbar, in order to evaluate the effect of sintering temperature.

2.2 Thermo-chemical treatment (functionalization)

Figure 2 Schematic process of titanium scaffold functionalization

Both the solid discs and the porous cylinders were soaked in 5M NaOH solution for 24 h at 60 °C. After gently washing the samples with distilled water, samples were immersed in calcium chloride (100 mM), with 5, 10, 50 or 100mM gallium nitrate at 40 °C for 24h. The samples were then heated at 5 °C/min until 600 °C and maintained 1 h at this temperature. In a final phase (water step), they were dipped in water at 80 °C for 24 h to facilitate the ionic release.

2.3 Scaffold characterization

2.3.1. Physicochemical characterization

The surface morphology of the Ti scaffolds was analyzed by scanning electron microscopy (Zeiss Neon 40, Carl Zeiss, Oberkochen, Germany). Sample shrinkage was evaluated by measuring the width and height of the samples before and after the sintering process using a digital caliper with 0.01 mm accuracy. The architecture of 3D-printed scaffolds was analyzed by X-ray computed microtomography (µCT, micro-CT Skyscan 1272, Bruker, Kontich, Belgium) at an isotropic pixel size of 3 µm. The percentage of interstitial carbon and oxygen was determinate by the elemental analyzer LECO (CS 200 and ON736).

2.3.2. Mechanical characterization

The scaffolds were subjected to a compression test, in accordance with the ISO standard 13314:2011 Cylindrical specimens printed with different porosity (50%, 60% and 70% according Gcode) sintered at two different temperatures (1150 °C and 1350 °C) were tested in an universal testing machine (Microtest machine EM1/20/FR, Microtest, Madrid, Spain).

2.4 Characterization of functionalized samples

2.4.1. Surface characterization

The inner and outer surface morphology and topography of porous treated-Ti samples were examined using a field emission scanning electron microscope (JEOL JSM-7001F). The chemical composition of the surfaces was analyzed using an energy dispersive X-ray analyzer (EDS, JEOL jsm-6400). The phases present on the treated-Ti surfaces were identified by a low angle X-ray diffraction (Bruker D8 advance, MA, USA) and A inVia™ Qontor® confocal Raman microscope (Renishaw Centrus 2957 T2, Gloucestershire, UK).

2.4.3. Evaluation of the apatite-forming ability

Simulated body fluid (SBF) prepared according the standard ISO 23317:2014 was used to study the formation of the apatite layer on Ti surfaces in vitro, as a method to predict its bioactivity in living bone. The treated-Ti samples were soaked in SBF and incubated at 37 °C for 3, 5 and 7 days. The hydroxyapatite formed on treated-Ti surfaces was evaluated by FESEM.

2.4.4 Antibacterial properties assay

The antibacterial properties were assessed using the agar diffusion test, commonly used procedure for studying the antibacterial action of the coated surfaces was followed. The assay was performed with both Staphylococcus epidermidis (S. epidermidis, CECT 231) and Staphylococcus aureus (S. aureus, CECT 59) as gram-positive and Pseudomonas aeruginosa (P. aeruginosa, CECT 110) and Escherichia coli (E. coli, CECT 101) as gram-negative organisms.

2.4.5 Cell response

For the adhesion the cells were seeded at a concentration of 50 000 cells/sample on treated Ti porous cylindrical samples and allowed to adhere for 6 h. For the proliferation studies, cells were cultured for 4 h, 3 days, 7 days, 14 days, 21 days, and 28 days changing the medium thrice a week. In the mineralization assay the cells were seeded under the same conditions described for the cell proliferation assays for 28 days. Then, the calcium deposits were stained Alizarin Red S (Sigma-Aldrich). Untreated Ti and Ti surfaces treated with the conventional treatment (TT) were used as controls.

3.   Results

3.1   Scaffold characterization

SEM images before and after the complete thermal treatment (1150 ºC) are shown in Figure 3. The microstructure of the scaffolds sintered at 1150 ºC showed good sintering between particles, with the formation of necks between adjacent particles due to solid-state diffusion (Figure 3 B). The global shrinkage of the scaffolds was determined by measuring the diameter and height before and after the thermal treatment, including the debinding and sintering steps. The calculated shrinkages after sintering at 1150 ºC and 1350 ºC were higher in the axial direction compared with the contraction in the transversal direction (Table 1). This is in agreement with previous results reported in the literature, with the larger contraction in the vertical direction being associated with the effect of the gravity force during sintering [15]. The global shrinkage increased with the sintering temperature due to the enhanced solid-state diffusion between powder grains, also in agreement with other studies with similar sintering conditions of time and temperature [15]–[18].
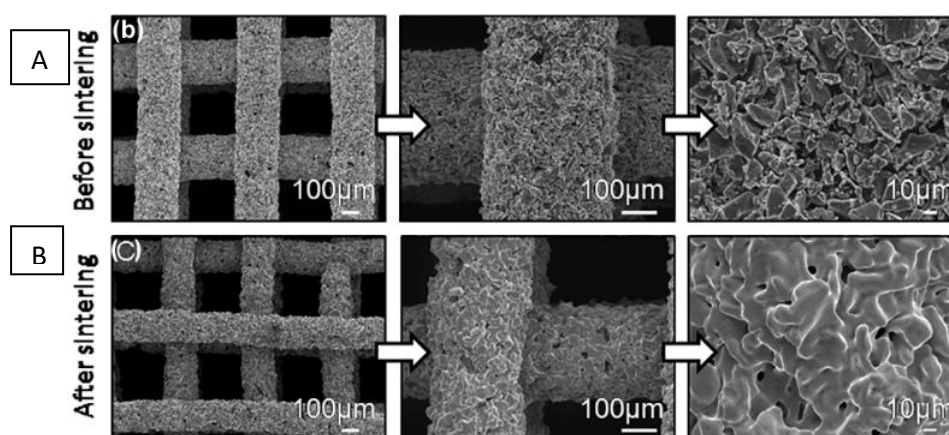

Figure 3 Images of 3D-printed scaffolds: A) SEM micrographs of the green body and B) SEM micrographs after the complete thermal treatment at 1150ºC.

Table 1. Characterization of the Ti scaffolds printed with different porosities (50%, 60% and 70%) and sintered at 1150 ºC and 1350 ºC. Real porosity obtained by MicroCT, percentage of scaffold shrinkage (diameter and height). Mechanical properties: Young's modulus (E) and Compressive strength (σc).

ID	Printing Porosity (%)	Sintering Temp. (ºC)	MicroCT Porosity (%)	Shrinkage (%)		E (GPa)	σ_c (MPa)
				Diameter	Height.		
50_13	50	1350	64±2	21±1	23±3	1.4±0.3	78±6
50_11	50	1150	65±4	15±1	14±2	1.2±0.1	36±7
60_13	60	1350	68±1	20±1	22±2	0.9±0.1	59±5
60_11	60	1150	69±3	14±1	15±2	0.9±0.1	28±4
70_13	70	1350	74±3	32±1	32±1	0.6±0.2	38±13
70_11	70	1150	78±3	23±1	24±2	0.5±0.1	16±6
70_V	70	25 (green)	78±1	0	0	-	0.9±0.1

All the scaffolds presented a bimodal porosity, with the scaffold pores resulting from the filament pattern design, and the pores in the struts produced during the debinding and the sintering process [19]. There are differences between the initial porosity designed and the real porosity (Table 1). This is due to the parameters modified during the printing process; however, knowing the value of this difference the porosity can be easily readjusted. The compressive strength gradually increased with the sintering temperature and with the reduction in porosity (Figure 4.A). Similar behaviour was observed for the Young's modulus (Figure 4.B), even though there are no statistically significant differences between the values measured at different sintering temperatures.
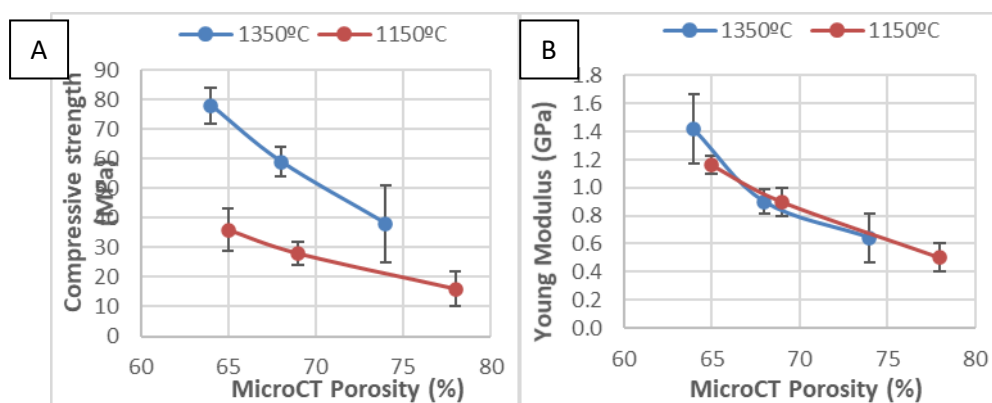
Figure 4 Evolution of mechanical properties of scaffolds with the porosity and temperature of sintering A) Young's modulus; B) Compressive strength

In all cases, the scaffold pore size was within the acceptable range to allow bone ingrowth, vascularization and transport of metabolic products, according to the literature [1], [20] and the mechanical properties of the prepared DIW Ti scaffolds are in the range of human trabecular bone [21]–[23].

3.2   Functionalization

3.2.1 Surface physicochemical characterization

A porous acicular feather-like structure was obtained with the thermochemical treatment in treated Ti surfaces (figure 5A). The thickness of the layer was similar (1.67 ± 0.38 µm). This value is similar to those obtained by Yamaguchi after similar treatment with gallium chloride [24]. The EDS analyses of the inner and outer surfaces of the porous structures showed that both Ga and Ca ions are present on the entire surface of the sample (Figure 5.B), confirming that the treatment penetrates the porous Ti structures. Raman analysis of porous Ti surfaces subjected only to the initial stages of the treatment (before thermal treatment) showed main bands at 270, 440 and 690 cm^{-1}, corresponding to both gallium hydrogen titanate or gallium-containing calcium hydrogen titanate [24], [25]. The diffraction peaks at 25° and 48° can be attributed to gallium-containing calcium titanate. While the rutile phase is shown with the diffraction peak at 37.5^O, anatase diffraction peak may overlap with the first Ga-Ca-T peak at 25° [24].
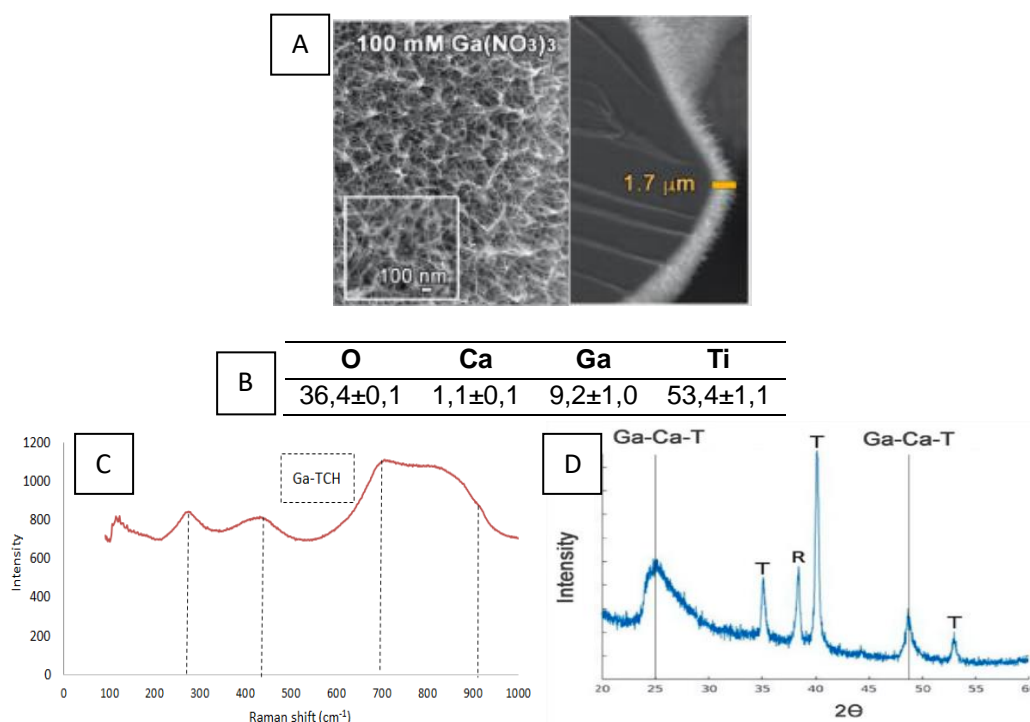

	O	Ca	Ga	Ti
B	36,4±0,1	1,1±0,1	9,2±1,0	53,4±1,1

Figure 5 Surface characterization of Ti scaffolds after thermo chemical treatment with 100mMGa(NO$_3$)$_3$: A) FESEM images of the feather-like structure of Ti surface and cross section. B) Elemental composition (wt.%) by EDS. C) Raman spectra of Ti samples without the thermal treatment. Ga-HT bands correspond to gallium hydrogen titanate or to gallium containing calcium hydrogen titanate. D) X-ray diffraction pattern of a treated Ti surface. Ga-Ca-T correspond to Ca titanate containing Ga, R correspond to rutile and T to α-Ti

3.2.2 Bioactivity analyse

The bone-bonding activity and the bioactivity degree of a surface can be assessed by examining the apatite formation on its surface in SBF [26]. Homogeneous coatings of apatite on the treated-Ti inner and outer surfaces were formed after 7 days of incubation in SBF (Figure 6A), with a good and continuous contact with the substrate (Figure 6B).

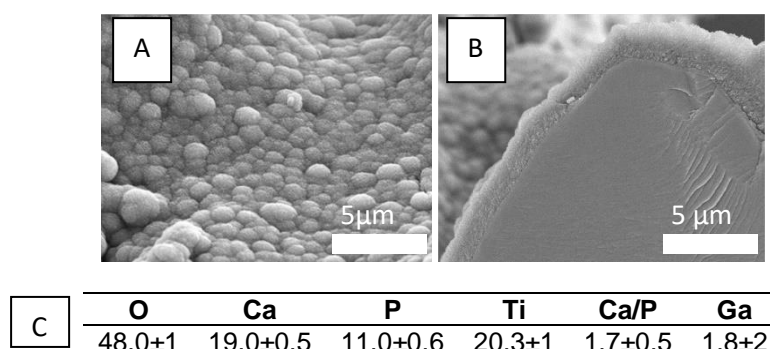| C	O	Ca	P	Ti	Ca/P	Ga
	48,0±1	19,0±0,5	11,0±0,6	20,3±1	1,7±0,5	1,8±2

Figure 6 FESEM micrographs (x4k) of A) surface and B) cross section of Ti scaffold treated and immersed in SBF for 7 days. C). EDS analysis (wt. %) of the coating formed after 7 days in SBF.

The EDS results indicated that the samples after being immersed in SBF generated a layer on the surface composed of calcium and phosphorus, most certainly in the form of calcium phosphates, with a Ca/P ratio of 1.7. According to the literature, this ratio agrees with that of the apatite [27] (Figure 6C).

3.2.3 Antibacterial properties

While surfaces used as controls (untreated porous Ti surfaces and treated with the conventional TT) did not induce an inhibition halo for any of the strains tested, Ga-treated Ti surfaces showed an inhibition halo for P. aeruginosa and E. coli (Figure 7 C and D).
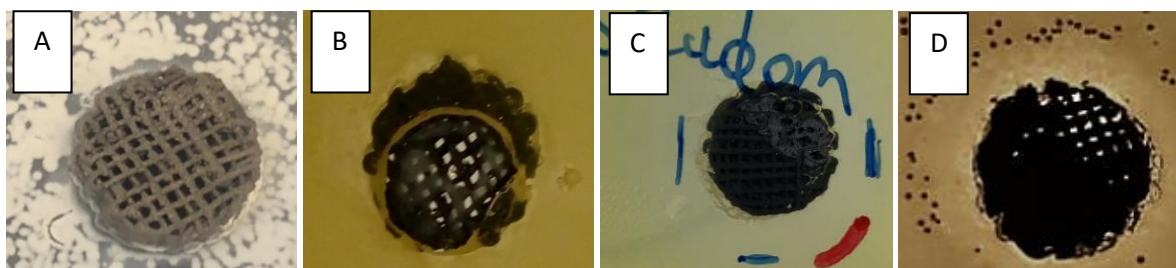

Figure 7 Photographs of the growth inhibition halo of A) Staphylococcus epidermidis, B) Staphylococcus aureus as gram-positive and C) Pseudomonas aeruginosa, D) Escherichia coli as gram-negative organisms on the Ti scaffolds after thermochemical treatment with 100 mM Ga(NO$_3$)$_3$.

In contrast to the results obtained for the gram-negative strains, no inhibitory effect of the Ga-containing Ti surfaces was acquired for the gram-positive bacteria S. epidermidis and S. aureus (Figure 7 A and b).The minimal inhibitory concentration (MIC) of a Ga salt for S. aureus is found between 375 and 2000 µg/ml and for S. epidermidis is established between 94 and 200 µg/ml [28]. Therefore, for bacterial inhibition, the Ga release should be greater than these values.

3.2.4. Adhesion, proliferation and mineralization

Cell count showed no significant differences in cell adhesion after 6 h of incubation between the controls (Ti and TT) and the treated Ti samples with Ga. Cells proliferated on all the substrates, but the rate of proliferation was different. Comparing both controls, proliferation on Ti treated with no Ga (TT) was lower than on the untreated Ti sample (Ti). Also compared to this last control, cell proliferation was lower on surfaces treated with Ga (Figure 8.A).
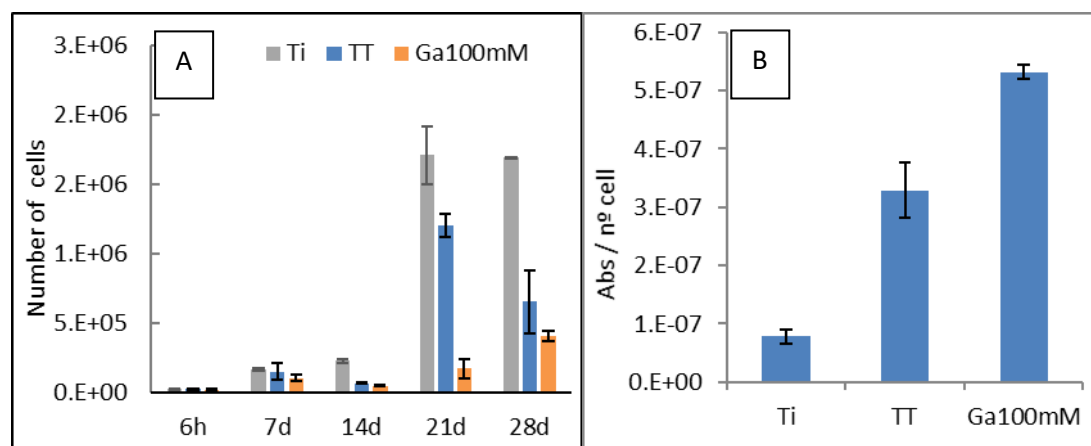
Figure 8 A) Cell adhesion and proliferation on the different treated Ti surfaces, Ti without treatment, TT with conventional treatment, Ga100mM with Ga. B) Quantification of calcium deposits produced by human osteoblast-like SaOS-2 cells on the Ga doped Ti surfaces after extracting Alizarin Red staining at 28 days of culture. Results were normalized vs their corresponding cell numbers.

During bone matrix maturation and mineralization, osteoblast proliferation is reduced [29]. Thus, while lower proliferation rates were obtained, mineralization was strongly promoted (Figure 8.B).

4.   Conclusions

Direct ink writing process was successfully developed allowing the manufacture of porous tridimensional scaffolds with controlled geometry and interconnected porosity. Adjustment of the sintering temperature allowed tuning the porosity of the titanium structures, and consequently the mechanical behavior. The sintered scaffolds presented an elastic modulus and compressive strength in the range of human cancellous bone. The suitability of applying the thermochemical treatment to porous structures produced by 3D-printing was confirmed. The incorporation of gallium nitrate in the process provoked the formation of a homogeneous layer of gallium-containing calcium titanate, anatase, and rutile on the inner and outer surfaces of microporous Ti scaffolds. This new chemical configuration on Ti surface promoted apatite precipitation. The presence of Ga on the Ti surfaces showed an antibacterial effect against gram-negative strains in the first hours and enhance the osteoinductive effect, promoting the differentiation and mineralization on Saos-2 cells

5.   Acknowledgments

6.   Bibliography

[1]   K. Alvarez and H. Nakajima, "Metallic Scaffolds for Bone Regeneration," Mater. 2009, pp. 790–832, 2009.

[2]   E. Vidal et al., "metals Titanium Sca ff olds by Direct Ink Writing : Fabrication and Functionalization to Guide Osteoblast Behavior."

[3]   A. Sidambe, "Biocompatibility of Advanced Manufactured Titanium Implants—A Review," Materials (Basel)., vol. 7, no. 12, pp. 8168–8188, 2014.

[4]   P. Jiang, Z. Ji, X. Zhang, Z. Liu, and X. Wang, "Recent advances in direct ink writing of electronic components and functional devices," Prog. Addit. Manuf., vol. 3, no. 1–2, pp. 65–86, 2018.

[5]   K. J. Bozic et al., "Comparative Epidemiology of Revision Arthroplasty: Failed THA Poses Greater Clinical and Economic Burdens Than Failed TKA.," Clin. Orthop. Relat. Res., vol. 473, no. 6, pp. 2131–2138, 2015.

[6]   M. Sundfeldt, L. V Carlsson, C. B. Johansson, P. Thomsen, and C. Gretzer, "Aseptic loosening, not only a question of wear: a review of different theories.," Acta Orthop., vol. 77, no. 2, pp. 177–197, 2006.

[7]   M. Geetha and R. Singh, "A. K. Asokamani and A.," K Gogia Ti based Biomater. Ultim. choice Orthop. Implant. Rev. Prog. Mater. Sci., vol. 54, no. 3 SRC-BaiduScholar FG-0, pp. 397–425, 2009.

[8]   J. Raphel, M. Holodniy, S. B. Goodman, and S. C. Heilshorn, "Multifunctional coatings to simultaneously promote osseointegration and prevent infection of orthopaedic implants," Biomaterials, vol. 84, pp. 301–314, 2016.

[9]   A. Rodríguez-Contreras et al., "Development of novel dual-action coatings with osteoinductive and antibacterial properties for 3D-printed titanium implants," Surf. Coatings Technol., vol. 403, no. August, p. 126381, 2020.

[10]   N. Kircheva and T. Dudev, "Gallium as an Antibacterial Agent: A DFT/SMD Study of the Ga3+/Fe3+ Competition for Binding Bacterial Siderophores," Inorg. Chem., vol. 59, no. 9, pp. 6242–6254, May 2020.

[11]   V. Nikolova, S. Angelova, N. Markova, and T. Dudev, "Gallium as a Therapeutic Agent: A Thermodynamic Evaluation of the Competition between Ga3+ and Fe3+ Ions in Metalloproteins," J. Phys. Chem. B, vol. 120, no. 9, pp. 2241–2248, Mar. 2016.

[12]   J. Liu, Z. Wu, H. He, K. Cai, H. Zhang, and L. Xu, "Gallium and silicon synergistically promote osseointegration of dental implant in patients with osteoporosis," Med. Hypotheses, vol. 103, pp. 35–38, 2017.

[13]   C. R. Chitambar, "Gallium-containing anticancer compounds.," Future Med. Chem., vol. 4, no. 10, pp. 1257–1272, Jun. 2012.

[14]   E. Verron et al., "Gallium modulates osteoclastic bone resorption in vitro without affecting osteoblasts.," Br. J. Pharmacol., vol. 159, no. 8, pp. 1681–1692, Apr. 2010.

[15]   F. E. Wiria, S. Maleksaeedi, and Z. He, "Manufacturing and characterization of porous titanium components," Prog. Cryst. Growth Charact. Mater., vol. 60, no. 3–4, pp. 94–98, 2014.

[16]   S. Maleksaeedi et al., "Toward 3D printed bioactive titanium scaffolds with bimodal pore size distribution for bone ingrowth," Procedia CIRP, vol. 5, pp. 158–163, 2013.

[17]   G. Gagg, E. Ghassemieh, and F. E. Wiria, "Effects of sintering temperature on morphology and mechanical characteristics of 3D printed porous titanium used as dental implant," Mater. Sci. Eng. C, vol. 33, no. 7, pp. 3858–3864, 2013.

[18]   J. P. Li, J. R. De Wijn, C. A. Van Blitterswijk, and K. De Groot, "The effect of scaffold architecture on properties of direct 3D fiber deposition of porous Ti6Al4V for orthopedic implants," J. Biomed. Mater. Res. - Part A, vol. 92, no. 1, pp. 33–42, 2010.

[19]   F. E. Wiria, J. Y. M. Shyan, P. N. Lim, F. G. C. Wen, J. F. Yeo, and T. Cao, "Printing of Titanium implant prototype," Mater. Des., vol. 31, no. SUPPL. 1, pp. S101–S105, 2010.

[20]   K. C. McGilvray et al., "Bony ingrowth potential of 3D-printed porous titanium alloy: a direct comparison of interbody cage materials in an in vivo ovine lumbar fusion model," Spine J., vol. 18, no. 7, pp. 1250–1260, 2018.

[21]   V. Karageorgiou and D. Kaplan, "Porosity of 3D biomaterial scaffolds and osteogenesis," Biomaterials, vol. 26, pp. 5474–5491, 2005.

[22]   F. Liu, D. Z. Zhang, P. Zhang, M. Zhao, and S. Jafar, "Mechanical properties of optimized diamond lattice structure for bone scaffolds fabricated via selective laser melting," Materials (Basel)., vol. 11, no. 3, 2018.

[23]   M. Geetha, A. K. Singh, R. Asokamani, and A. K. Gogia, "Ti based biomaterials, the ultimate choice for orthopaedic implants - A review," Prog. Mater. Sci., vol. 54, no. 3, pp. 397–425, 2009.

[24]   S. Yamaguchi et al., "Two-in-One Biointerfaces—Antimicrobial and Bioactive Nanoporous Gallium Titanate Layers for Titanium Implants," Nanomaterials, 2017.

[25]   T. Kizuki, H. Takadama, T. Matsushita, T. Nakamura, and T. Kokubo, "Preparation of bioactive Ti metal surface enriched with calcium ions by chemical treatment," Acta Biomater., vol. 6, no. 7, pp. 2836–2842, 2010.

[26]   T. Kokubo and H. Takadama, "How useful is SBF in predicting in vivo bone bioactivity?," Biomaterials, vol. 27, no. 15, pp. 2907–2915, May 2006.

[27]   S. Raynaud, E. Champion, D. Bernache-Assollant, and P. Thomas, "Calcium phosphate apatites with variable Ca/P atomic ratio I. Synthesis, characterisation and thermal stability of powders," Biomaterials, vol. 23, no. 4, pp. 1065–1072, 2002.

[28]   D. Baldoni, A. Steinhuber, W. Zimmerli, and A. Trampuz, "In vitro activity of gallium maltolate against staphylococci in logarithmic, stationary, and biofilm growth phases: Comparison of conventional and calorimetric susceptibility testing methods," Antimicrob. Agents Chemother., vol. 54, no. 1, pp. 157–163, 2010.

[29]   J. Chen et al., "99Tc-MDP-induced human osteoblast proliferation, differentiation and expression of osteoprotegerin," Mol. Med. Rep., vol. 16, no. 2, pp. 1801–1809, 2017.